

Partial wave analysis of $\psi(3686) \rightarrow K^+ K^- \eta$

M. Ablikim,¹ M. N. Achasov,^{10,d} P. Adlarson,⁵⁹ S. Ahmed,¹⁵ M. Albrecht,⁴ M. Alekseev,^{58a,58c} A. Amoroso,^{58a,58c} F. F. An,¹ Q. An,^{55,43} Y. Bai,⁴² O. Bakina,²⁷ R. Baldini Ferroli,^{23a} I. Balossino,^{24a} Y. Ban,³⁵ K. Begzsuren,²⁵ J. V. Bennett,⁵ N. Berger,²⁶ M. Bertani,^{23a} D. Bettoni,^{24a} F. Bianchi,^{58a,58c} J. Biernat,⁵⁹ J. Bloms,⁵² I. Boyko,²⁷ R. A. Briere,⁵ H. Cai,⁶⁰ X. Cai,^{1,43} A. Calcaterra,^{23a} G. F. Cao,^{1,47} N. Cao,^{1,47} S. A. Cetin,^{46b} J. Chai,^{58c} J. F. Chang,^{1,43} W. L. Chang,^{1,47} G. Chelkov,^{27,b,c} D. Y. Chen,⁶ G. Chen,¹ H. S. Chen,^{1,47} J. C. Chen,¹ M. L. Chen,^{1,43} S. J. Chen,³³ Y. B. Chen,^{1,43} W. Cheng,^{58c} G. Cibinetto,^{24a} F. Cossio,^{58c} X. F. Cui,³⁴ H. L. Dai,^{1,43} J. P. Dai,^{38,h} X. C. Dai,^{1,47} A. Dbeysi,¹⁵ D. Dedovich,²⁷ Z. Y. Deng,¹ A. Denig,²⁶ I. Denysenko,²⁷ M. Destefanis,^{58a,58c} F. De Mori,^{58a,58c} Y. Ding,³¹ C. Dong,³⁴ J. Dong,^{1,43} L. Y. Dong,^{1,47} M. Y. Dong,^{1,43,47} Z. L. Dou,³³ S. X. Du,⁶³ J. Z. Fan,⁴⁵ J. Fang,^{1,43} S. S. Fang,^{1,47} Y. Fang,¹ R. Farinelli,^{24a,24b} L. Fava,^{58b,58c} F. Feldbauer,⁴ G. Felici,^{23a} C. Q. Feng,^{55,43} M. Fritsch,⁴ C. D. Fu,¹ Y. Fu,¹ Q. Gao,¹ X. L. Gao,^{55,43} Y. Gao,⁴⁵ Y. Gao,⁵⁶ Y. G. Gao,⁶ Z. Gao,^{55,43} B. Garillon,²⁶ I. Garzia,^{24a} E. M. Gersabeck,⁵⁰ A. Gilman,⁵¹ K. Goetzen,¹¹ L. Gong,³⁴ W. X. Gong,^{1,43} W. Gradl,²⁶ M. Greco,^{58a,58c} L. M. Gu,³³ M. H. Gu,^{1,43} S. Gu,² Y. T. Gu,¹³ A. Q. Guo,²² L. B. Guo,³² R. P. Guo,³⁶ Y. P. Guo,²⁶ A. Guskov,²⁷ S. Han,⁶⁰ X. Q. Hao,¹⁶ F. A. Harris,⁴⁸ K. L. He,^{1,47} F. H. Heinsius,⁴ T. Held,⁴ Y. K. Heng,^{1,43,47} M. Himmelreich,^{11,g} Y. R. Hou,⁴⁷ Z. L. Hou,¹ H. M. Hu,^{1,47} J. F. Hu,^{38,h} T. Hu,^{1,43,47} Y. Hu,¹ G. S. Huang,^{55,43} J. S. Huang,¹⁶ X. T. Huang,³⁷ X. Z. Huang,³³ N. Huesken,⁵² T. Hussain,⁵⁷ W. Ikegami Andersson,⁵⁹ W. Imoehl,²² M. Irshad,^{55,43} Q. Ji,¹ Q. P. Ji,¹⁶ X. B. Ji,^{1,47} X. L. Ji,^{1,43} H. L. Jiang,³⁷ X. S. Jiang,^{1,43,47} X. Y. Jiang,³⁴ J. B. Jiao,³⁷ Z. Jiao,¹⁸ D. P. Jin,^{1,43,47} S. Jin,³³ Y. Jin,⁴⁹ T. Johansson,⁵⁹ N. Kalantar-Nayestanaki,²⁹ X. S. Kang,³¹ R. Kappert,²⁹ M. Kavatsyuk,²⁹ B. C. Ke,¹ I. K. Keshk,⁴ A. Khokkaz,⁵² P. Kiese,²⁶ R. Kiuchi,¹ R. Kliemt,¹¹ L. Koch,²⁸ O. B. Kolcu,^{46b,f} B. Kopf,⁴ M. Kuemmel,⁴ M. Kuessner,⁴ A. Kupsc,⁵⁹ M. Kurth,¹ M. G. Kurth,^{1,47} W. Kühn,²⁸ J. S. Lange,²⁸ P. Larin,¹⁵ L. Lavezzi,^{58c} H. Leithoff,²⁶ T. Lenz,²⁶ C. Li,⁵⁹ Cheng Li,^{55,43} D. M. Li,⁶³ F. Li,^{1,43} F. Y. Li,³⁵ G. Li,¹ H. B. Li,^{1,47} H. J. Li,^{9,j} J. C. Li,¹ J. W. Li,⁴¹ Ke Li,¹ L. K. Li,¹ Lei Li,³ P. L. Li,^{55,43} P. R. Li,³⁰ Q. Y. Li,³⁷ W. D. Li,^{1,47} W. G. Li,¹ X. H. Li,^{55,43} X. L. Li,³⁷ X. N. Li,^{1,43} Z. B. Li,⁴⁴ Z. Y. Li,⁴⁴ H. Liang,^{55,43} H. Liang,^{1,47} Y. F. Liang,⁴⁰ Y. T. Liang,²⁸ G. R. Liao,¹² L. Z. Liao,^{1,47} J. Libby,²¹ C. X. Lin,⁴⁴ D. X. Lin,¹⁵ Y. J. Lin,¹³ B. Liu,^{38,h} B. J. Liu,¹ C. X. Liu,¹ D. Liu,^{55,43} D. Y. Liu,^{38,h} F. H. Liu,³⁹ Fang Liu,¹ Feng Liu,⁶ H. B. Liu,¹³ H. M. Liu,^{1,47} Huanhuan Liu,¹ Huihui Liu,¹⁷ J. B. Liu,^{55,43} J. Y. Liu,^{1,47} K. Y. Liu,³¹ Ke Liu,⁶ L. Y. Liu,¹³ Q. Liu,⁴⁷ S. B. Liu,^{55,43} T. Liu,^{1,47} X. Liu,³⁰ X. Y. Liu,^{1,47} Y. B. Liu,³⁴ Z. A. Liu,^{1,43,47} Zhiqing Liu,³⁷ Y. F. Long,³⁵ X. C. Lou,^{1,43,47} H. J. Lu,¹⁸ J. D. Lu,^{1,47} J. G. Lu,^{1,43} Y. Lu,¹ Y. P. Lu,^{1,43} C. L. Luo,³² M. X. Luo,⁶² P. W. Luo,⁴⁴ T. Luo,^{9,j} X. L. Luo,^{1,43} S. Lusso,^{58c} X. R. Lyu,⁴⁷ F. C. Ma,³¹ H. L. Ma,¹ L. L. Ma,³⁷ M. M. Ma,^{1,47} Q. M. Ma,¹ X. N. Ma,³⁴ X. X. Ma,^{1,47} X. Y. Ma,^{1,43} Y. M. Ma,³⁷ F. E. Maas,¹⁵ M. Maggiora,^{58a,58c} S. Maldaner,²⁶ S. Malde,⁵³ Q. A. Malik,⁵⁷ A. Mangoni,^{23b} Y. J. Mao,³⁵ Z. P. Mao,¹ S. Marcello,^{58a,58c} Z. X. Meng,⁴⁹ J. G. Messchendorp,²⁹ G. Mezzadri,^{24a} J. Min,^{1,43} T. J. Min,³³ R. E. Mitchell,²² X. H. Mo,^{1,43,47} Y. J. Mo,⁶ C. Morales Morales,¹⁵ N. Yu. Muchnoi,^{10,d} H. Muramatsu,⁵¹ A. Mustafa,⁴ S. Nakhoul,^{11,g} Y. Nefedov,²⁷ F. Nerling,^{11,g} I. B. Nikolaev,^{10,d} Z. Ning,^{1,43} S. Nisar,^{8,k} S. L. Niu,^{1,43} S. L. Olsen,⁴⁷ Q. Ouyang,^{1,43,47} S. Pacetti,^{23b} Y. Pan,^{55,43} M. Papenbrock,⁵⁹ P. Patteri,^{23a} M. Pelizaeus,⁴ H. P. Peng,^{55,43} K. Peters,^{11,g} J. Pettersson,⁵⁹ J. L. Ping,³² R. G. Ping,^{1,47} A. Pitka,⁴ R. Poling,⁵¹ V. Prasad,^{55,43} H. R. Qi,² M. Qi,³³ T. Y. Qi,² S. Qian,^{1,43} C. F. Qiao,⁴⁷ N. Qin,⁶⁰ X. P. Qin,¹³ X. S. Qin,⁴ Z. H. Qin,^{1,43} J. F. Qiu,¹ S. Q. Qu,³⁴ K. H. Rashid,^{57,i} K. Ravindran,²¹ C. F. Redmer,²⁶ M. Richter,⁴ A. Rivetti,^{58c} V. Rodin,²⁹ M. Rolo,^{58c} G. Rong,^{1,47} Ch. Rosner,¹⁵ M. Rump,⁵² A. Sarantsev,^{27,e} M. Savrić,^{24b} Y. Schelhaas,²⁶ K. Schoenning,⁵⁹ W. Shan,¹⁹ X. Y. Shan,^{55,43} M. Shao,^{55,43} C. P. Shen,² P. X. Shen,³⁴ X. Y. Shen,^{1,47} H. Y. Sheng,¹ X. Shi,^{1,43} X. D. Shi,^{55,43} J. J. Song,³⁷ Q. Q. Song,^{55,43} X. Y. Song,¹ S. Sosio,^{58a,58c} C. Sowa,⁴ S. Spataro,^{58a,58c} F. F. Sui,³⁷ G. X. Sun,¹ J. F. Sun,¹⁶ L. Sun,⁶⁰ S. S. Sun,^{1,47} X. H. Sun,¹ Y. J. Sun,^{55,43} Y. K. Sun,^{55,43} Y. Z. Sun,¹ Z. J. Sun,^{1,43} Z. T. Sun,¹ Y. T. Tan,^{55,43} C. J. Tang,⁴⁰ G. Y. Tang,¹ X. Tang,¹ V. Thoren,⁵⁹ B. Tsednee,²⁵ I. Uman,^{46d} B. Wang,¹ B. L. Wang,⁴⁷ C. W. Wang,³³ D. Y. Wang,³⁵ K. Wang,^{1,43} L. L. Wang,¹ L. S. Wang,¹ M. Wang,³⁷ M. Z. Wang,³⁵ Meng Wang,^{1,47} P. L. Wang,¹ R. M. Wang,⁶¹ W. P. Wang,^{55,43} X. Wang,³⁵ X. F. Wang,¹ X. L. Wang,^{9,j} Y. Wang,^{55,43} Y. Wang,⁴⁴ Y. F. Wang,^{1,43,47} Z. Wang,^{1,43} Z. G. Wang,^{1,43} Z. Y. Wang,¹ Zongyuan Wang,^{1,47} T. Weber,⁴ D. H. Wei,¹² P. Weidenkaff,²⁶ H. W. Wen,³² S. P. Wen,¹ U. Wiedner,⁴ G. Wilkinson,⁵³ M. Wolke,⁵⁹ L. H. Wu,¹ L. J. Wu,^{1,47} Z. Wu,^{1,43} L. Xia,^{55,43} Y. Xia,²⁰ S. Y. Xiao,¹ Y. J. Xiao,^{1,47} Z. J. Xiao,³² Y. G. Xie,^{1,43} Y. H. Xie,⁶ T. Y. Xing,^{1,47} X. A. Xiong,^{1,47} Q. L. Xiu,^{1,43} G. F. Xu,¹ J. J. Xu,³³ L. Xu,¹ Q. J. Xu,¹⁴ W. Xu,^{1,47} X. P. Xu,⁴¹ F. Yan,⁵⁶ L. Yan,^{58a,58c} W. B. Yan,^{55,43} W. C. Yan,² Y. H. Yan,²⁰ H. J. Yang,^{38,h} H. X. Yang,¹ L. Yang,⁶⁰ R. X. Yang,^{55,43} S. L. Yang,^{1,47} Y. H. Yang,³³ Y. X. Yang,¹² Yifan Yang,^{1,47} Z. Q. Yang,²⁰ M. Ye,^{1,43} M. H. Ye,⁷ J. H. Yin,¹ Z. Y. You,⁴⁴ B. X. Yu,^{1,43,47} C. X. Yu,³⁴ J. S. Yu,²⁰ T. Yu,⁵⁶ C. Z. Yuan,^{1,47} X. Q. Yuan,³⁵ Y. Yuan,¹ A. Yuncu,^{46b,a} A. A. Zafar,⁵⁷ Y. Zeng,²⁰ B. X. Zhang,¹ B. Y. Zhang,^{1,43} C. C. Zhang,¹ D. H. Zhang,¹ H. H. Zhang,⁴⁴ H. Y. Zhang,^{1,43} J. Zhang,^{1,47} J. L. Zhang,⁶¹ J. Q. Zhang,⁴ J. W. Zhang,^{1,43,47} J. Y. Zhang,¹ J. Z. Zhang,^{1,47} K. Zhang,^{1,47} L. Zhang,⁴⁵ S. F. Zhang,³³ T. J. Zhang,^{38,h} X. Y. Zhang,³⁷ Y. Zhang,^{55,43} Y. H. Zhang,^{1,43} Y. T. Zhang,^{55,43} Yang Zhang,¹ Yao Zhang,¹ Yi Zhang,^{9,j} Yu Zhang,⁴⁷ Z. H. Zhang,⁶ Z. P. Zhang,⁵⁵ Z. Y. Zhang,⁶⁰ G. Zhao,¹ J. W. Zhao,^{1,43} J. Y. Zhao,^{1,47}

J. Z. Zhao,^{1,43} Lei Zhao,^{55,43} Ling Zhao,¹ M. G. Zhao,³⁴ Q. Zhao,¹ S. J. Zhao,⁶³ T. C. Zhao,¹ Y. B. Zhao,^{1,43} Z. G. Zhao,^{55,43}
 A. Zhemchugov,^{27,b} B. Zheng,⁵⁶ J. P. Zheng,^{1,43} Y. Zheng,³⁵ Y. H. Zheng,⁴⁷ B. Zhong,³² L. Zhou,^{1,43} L. P. Zhou,^{1,47}
 Q. Zhou,^{1,47} X. Zhou,⁶⁰ X. K. Zhou,⁴⁷ X. R. Zhou,^{55,43} Xiaoyu Zhou,²⁰ Xu Zhou,²⁰ A. N. Zhu,^{1,47} J. Zhu,³⁴ J. Zhu,⁴⁴
 K. Zhu,¹ K. J. Zhu,^{1,43,47} S. H. Zhu,⁵⁴ W. J. Zhu,³⁴ X. L. Zhu,⁴⁵ Y. C. Zhu,^{55,43} Y. S. Zhu,^{1,47} Z. A. Zhu,^{1,47} J. Zhuang,^{1,43}
 B. S. Zou,¹ and J. H. Zou¹

(BESIII Collaboration)

- ¹*Institute of High Energy Physics, Beijing 100049, People's Republic of China*
²*Beihang University, Beijing 100191, People's Republic of China*
³*Beijing Institute of Petrochemical Technology, Beijing 102617, People's Republic of China*
⁴*Bochum Ruhr-University, D-44780 Bochum, Germany*
⁵*Carnegie Mellon University, Pittsburgh, Pennsylvania 15213, USA*
⁶*Central China Normal University, Wuhan 430079, People's Republic of China*
⁷*China Center of Advanced Science and Technology, Beijing 100190, People's Republic of China*
⁸*COMSATS University Islamabad, Lahore Campus, Defence Road, Off Raiwind Road, 54000 Lahore, Pakistan*
⁹*Fudan University, Shanghai 200443, People's Republic of China*
¹⁰*G.I. Budker Institute of Nuclear Physics SB RAS (BINP), Novosibirsk 630090, Russia*
¹¹*GSI Helmholtzcentre for Heavy Ion Research GmbH, D-64291 Darmstadt, Germany*
¹²*Guangxi Normal University, Guilin 541004, People's Republic of China*
¹³*Guangxi University, Nanning 530004, People's Republic of China*
¹⁴*Hangzhou Normal University, Hangzhou 310036, People's Republic of China*
¹⁵*Helmholtz Institute Mainz, Johann-Joachim-Becher-Weg 45, D-55099 Mainz, Germany*
¹⁶*Henan Normal University, Xinxiang 453007, People's Republic of China*
¹⁷*Henan University of Science and Technology, Luoyang 471003, People's Republic of China*
¹⁸*Huangshan College, Huangshan 245000, People's Republic of China*
¹⁹*Hunan Normal University, Changsha 410081, People's Republic of China*
²⁰*Hunan University, Changsha 410082, People's Republic of China*
²¹*Indian Institute of Technology Madras, Chennai 600036, India*
²²*Indiana University, Bloomington, Indiana 47405, USA*
^{23a}*INFN Laboratori Nazionali di Frascati, I-00044 Frascati, Italy*
^{23b}*INFN and University of Perugia, I-06100 Perugia, Italy*
^{24a}*INFN Sezione di Ferrara, I-44122 Ferrara, Italy*
^{24b}*University of Ferrara, I-44122 Ferrara, Italy*
²⁵*Institute of Physics and Technology, Peace Ave. 54B, Ulaanbaatar 13330, Mongolia*
²⁶*Johannes Gutenberg University of Mainz, Johann-Joachim-Becher-Weg 45, D-55099 Mainz, Germany*
²⁷*Joint Institute for Nuclear Research, 141980 Dubna, Moscow region, Russia*
²⁸*Justus-Liebig-Universitaet Giessen, II. Physikalisches Institut, Heinrich-Buff-Ring 16, D-35392 Giessen, Germany*
²⁹*KVI-CART, University of Groningen, NL-9747 AA Groningen, Netherlands*
³⁰*Lanzhou University, Lanzhou 730000, People's Republic of China*
³¹*Liaoning University, Shenyang 110036, People's Republic of China*
³²*Nanjing Normal University, Nanjing 210023, People's Republic of China*
³³*Nanjing University, Nanjing 210093, People's Republic of China*
³⁴*Nankai University, Tianjin 300071, People's Republic of China*
³⁵*Peking University, Beijing 100871, People's Republic of China*
³⁶*Shandong Normal University, Jinan 250014, People's Republic of China*
³⁷*Shandong University, Jinan 250100, People's Republic of China*
³⁸*Shanghai Jiao Tong University, Shanghai 200240, People's Republic of China*
³⁹*Shanxi University, Taiyuan 030006, People's Republic of China*
⁴⁰*Sichuan University, Chengdu 610064, People's Republic of China*
⁴¹*Soochow University, Suzhou 215006, People's Republic of China*
⁴²*Southeast University, Nanjing 211100, People's Republic of China*
⁴³*State Key Laboratory of Particle Detection and Electronics, Beijing 100049, Hefei 230026, People's Republic of China*
⁴⁴*Sun Yat-Sen University, Guangzhou 510275, People's Republic of China*
⁴⁵*Tsinghua University, Beijing 100084, People's Republic of China*
^{46a}*Ankara University, 06100 Tandogan, Ankara, Turkey*

- ^{46b}*Istanbul Bilgi University, 34060 Eyup, Istanbul, Turkey*
^{46c}*Uludag University, 16059 Bursa, Turkey*
^{46d}*Near East University, Nicosia, North Cyprus, Mersin 10, Turkey*
⁴⁷*University of Chinese Academy of Sciences, Beijing 100049, People's Republic of China*
⁴⁸*University of Hawaii, Honolulu, Hawaii 96822, USA*
⁴⁹*University of Jinan, Jinan 250022, People's Republic of China*
⁵⁰*University of Manchester, Oxford Road, Manchester M13 9PL, United Kingdom*
⁵¹*University of Minnesota, Minneapolis, Minnesota 55455, USA*
⁵²*University of Muenster, Wilhelm-Klemm-Str. 9, 48149 Muenster, Germany*
⁵³*University of Oxford, Keble Rd, Oxford, United Kingdom OX13RH*
⁵⁴*University of Science and Technology Liaoning, Anshan 114051, People's Republic of China*
⁵⁵*University of Science and Technology of China, Hefei 230026, People's Republic of China*
⁵⁶*University of South China, Hengyang 421001, People's Republic of China*
⁵⁷*University of the Punjab, Lahore-54590, Pakistan*
^{58a}*University of Turin, I-10125 Turin, Italy*
^{58b}*University of Eastern Piedmont, I-15121 Alessandria, Italy*
^{58c}*INFN, I-10125 Turin, Italy*
⁵⁹*Uppsala University, Box 516, SE-75120 Uppsala, Sweden*
⁶⁰*Wuhan University, Wuhan 430072, People's Republic of China*
⁶¹*Xinyang Normal University, Xinyang 464000, People's Republic of China*
⁶²*Zhejiang University, Hangzhou 310027, People's Republic of China*
⁶³*Zhengzhou University, Zhengzhou 450001, People's Republic of China*



(Received 19 December 2019; accepted 12 February 2020; published 28 February 2020)

Using a sample of $(448.1 \pm 2.9) \times 10^6$ $\psi(3686)$ events collected with the BESIII detector, we perform the first partial wave analysis of $\psi(3686) \rightarrow K^+K^-\eta$. In addition to the well established states, $\phi(1020)$, $\phi(1680)$, and $K_3^*(1780)$, contributions from $X(1750)$, $\rho(2150)$, $\rho_3(2250)$, and $K_2^*(1980)$ are also observed. The $X(1750)$ state is determined to be a 1^{--} resonance. The simultaneous observation of the $\phi(1680)$ and $X(1750)$ indicates that the $X(1750)$, with previous observations in photoproduction, is distinct from the $\phi(1680)$. The masses, widths, branching fractions of $\psi(3686) \rightarrow K^+K^-\eta$, and the intermediate resonances are also measured.

DOI: [10.1103/PhysRevD.101.032008](https://doi.org/10.1103/PhysRevD.101.032008)

I. INTRODUCTION

Within the framework of the relativistic quark model [1], a spectrum similar to that of a heavy quarkonia is expected for the strangeonium ($s\bar{s}$) sector [2]. A comprehensive study of the strangeonium spectrum is useful to test the theoretical models and also in the search for light exotica (resonances that are not dominantly $q\bar{q}$ states, often with nonexotic quantum numbers). Strangeonia have been studied in different experiments, such as the study of the initial-state radiation [3–7], J/ψ

^aAlso at Bogazici University, 34342 Istanbul, Turkey.

^bAlso at the Moscow Institute of Physics and Technology, Moscow 141700, Russia.

^cAlso at the Functional Electronics Laboratory, Tomsk State University, Tomsk 634050, Russia.

^dAlso at the Novosibirsk State University, Novosibirsk 630090, Russia.

^eAlso at the NRC "Kurchatov Institute", PNPI, 188300 Gatchina, Russia.

^fAlso at Istanbul Arel University, 34295 Istanbul, Turkey.

^gAlso at Goethe University Frankfurt, 60323 Frankfurt am Main, Germany.

^hAlso at Key Laboratory for Particle Physics, Astrophysics and Cosmology, Ministry of Education; Shanghai Key Laboratory for Particle Physics and Cosmology; Institute of Nuclear and Particle Physics, Shanghai 200240, People's Republic of China.

ⁱAlso at Government College Women University, Sialkot - 51310 Punjab, Pakistan.

^jAlso at Key Laboratory of Nuclear Physics and Ion-beam Application (MOE) and Institute of Modern Physics, Fudan University, Shanghai 200443, People's Republic of China.

^kAlso at Harvard University, Department of Physics, Cambridge, Massachusetts, 02138, USA.

Published by the American Physical Society under the terms of the [Creative Commons Attribution 4.0 International license](https://creativecommons.org/licenses/by/4.0/). Further distribution of this work must maintain attribution to the author(s) and the published article's title, journal citation, and DOI. Funded by SCOAP³.

and $\psi(3686)$ decays [8–11], and photoproduction data [12–15]. However, the strangeonium spectrum is much less well understood, and only a few states have been established. Given the unsatisfactory knowledge of strangeonium states, a search for missing states predicted by the relativistic quark model is necessary to improve the knowledge of the strangeonium spectrum. As proposed in Ref. [16], the available high statistics data collected by the BESIII experiment offer excellent opportunities to explore the strangeonium spectrum through J/ψ and $\psi(3686)$ decays.

Using 1.06×10^8 $\psi(3686)$ events collected in 2009, BESIII reported a study of $\psi(3686) \rightarrow K^+K^-\pi^0$ and $\psi(3686) \rightarrow K^+K^-\eta$ [9]. Two structures are evident in the K^+K^- mass spectrum in $\psi(3686) \rightarrow K^+K^-\eta$, and further study of these structures with larger data samples is needed. The BESIII experiment has collected a sample of $(448.1 \pm 2.9) \times 10^6$ $\psi(3686)$ events [17], about 4 times larger than the sample used in Ref. [9], which enables such a reexamination. In addition, the larger statistics also allows for a study of the K^* states in the $K^\pm\eta$ mass spectrum. In this paper, we present a partial wave analysis (PWA) of $\psi(3686) \rightarrow K^+K^-\eta$, which investigates the intermediate states in both mass spectra.

II. BESIII DETECTOR AND MONTE CARLO SIMULATION

The BESIII detector is a magnetic spectrometer [18] located at the Beijing Electron Positron Collider (BEPCII) [19]. The cylindrical core of the BESIII detector consists of a helium-based multilayer drift chamber (MDC), a plastic scintillator time-of-flight system (TOF), and a CsI(Tl) electromagnetic calorimeter (EMC), which are all enclosed in a superconducting solenoidal magnet providing a 1.0 T magnetic field. The solenoid is supported by an octagonal flux-return yoke with resistive plate counter muon identifier modules interleaved with steel. The acceptance of charged particles and photons is 93% over a 4π solid angle. The charged-particle momentum resolution at 1 GeV/ c is 0.5%, and the dE/dx resolution is 6% for the electrons from Bhabha scattering. The EMC measures photon energies with a resolution of 2.5% (5%) at 1 GeV in the barrel (end cap) region. The time resolution of the TOF barrel part is 68 ps, while that of the end cap part is 110 ps.

Simulated samples produced with the GEANT4-based [20] Monte Carlo (MC) package, which includes the geometric description of the BESIII detector and the detector response, are used to determine the detection efficiency and to estimate the backgrounds. The simulation includes the beam energy spread and initial state radiation (ISR) in the e^+e^- annihilations modeled with the generator KKMC [21]. The inclusive MC sample consists of the production of the J/ψ resonance, and the continuum processes incorporated in KKMC [21]. The known decay modes are modeled with EVTGEN [22] using branching fractions taken

from the Particle Data Group [23], and the remaining unknown decays from the charmonium states with LUNDCHARM [24]. Final state radiation (FSR) from charged final-state particles is incorporated with the PHOTOS package [25].

III. EVENT SELECTION

Candidate events for $\psi(3686) \rightarrow K^+K^-\eta, \eta \rightarrow \gamma\gamma$ are required to have two charged tracks with opposite charge and at least two photons. Charged tracks in the polar angle (θ) range $|\cos\theta| < 0.93$ are reconstructed using hits in the MDC. Charged tracks are required to pass within ± 10 cm of the interaction point (IP) in the direction parallel to the beam and within 1 cm of the IP in the plane perpendicular to the beam. The combined information from the energy loss (dE/dx) measured in the MDC and the flight time in the TOF is used to form particle identification (PID) confidence levels for the π , K and p hypotheses. A charged track is identified as a kaon if its PID confidence level for the kaon hypothesis is larger than that for the pion and proton hypotheses. Both charged tracks for candidate events are required to be identified as kaons. Photon candidates are required to have an energy deposit in the EMC of at least 25 MeV in the barrel ($|\cos\theta| < 0.80$) or 50 MeV in the end caps ($0.86 < |\cos\theta| < 0.92$). To eliminate showers from charged particles, photon candidates must have an opening angle of at least 10° from all charged tracks. To suppress electronic noise and showers unrelated to the event, the EMC time difference from the event start time is required to be within [0, 700] ns.

A four-constraint (4C) kinematic fit is performed under the $K^+K^-\gamma\gamma$ hypothesis, where the total measured four momentum is constrained to the four momentum of the initial e^+e^- system. For events with more than two photon candidates, the combination with the smallest χ^2 is retained. To reject possible background contributions with more or fewer photons, the 4C kinematic fits are also performed under the hypotheses $K^+K^-\gamma$ and $K^+K^-\gamma\gamma\gamma$. Only events for which the χ^2 value for the signal hypothesis is less than 30 and also less than the χ^2 values for the background hypotheses are retained.

The $\gamma\gamma$ invariant mass distribution for events that survive the selection criteria is shown in Fig. 1(a), where a clear η peak is observed. The K^+K^- mass spectrum is displayed in Fig. 1(b) after requiring $|M(\gamma\gamma) - m_\eta| < 0.02$ GeV/ c^2 , where m_η is the world average mass of the η meson [23]. The two narrow, significant peaks correspond to the $\phi(1020)$ and J/ψ , respectively, that come from decays of $\psi(3686) \rightarrow \phi\eta$ and $\psi(3686) \rightarrow J/\psi\eta$ with the resonances then decaying to K^+K^- . The $\phi(1020)$ and J/ψ are very well established, and the region between $m_{\phi(1020)}$ and $m_{J/\psi}$ is more interesting. In this analysis, only the events in the region $1.20 < M(K^+K^-) < 3.05$ GeV/ c^2 are used.

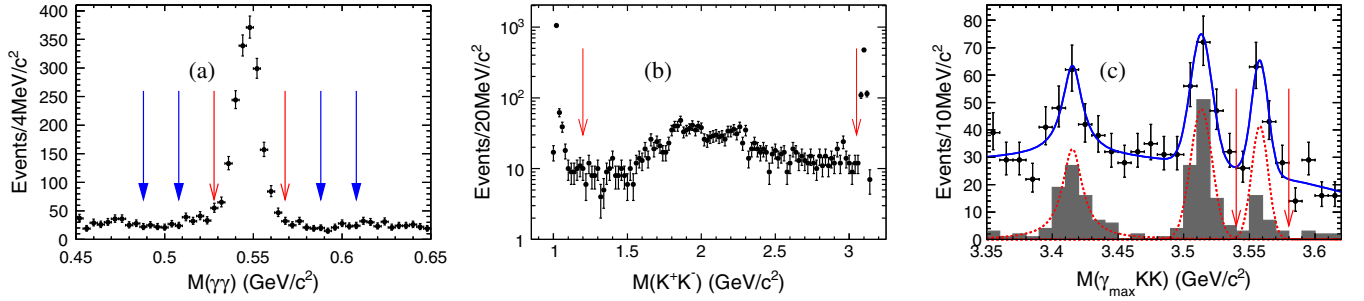


FIG. 1. (a) The $\gamma\gamma$ invariant mass spectrum for the data. The red arrows show the η signal region, while the blue arrows with solid arrowheads show the η sidebands. (b) The global K^+K^- invariant mass distribution for the data. Arrows show the requirement used to exclude events from $\phi(1020)$ and J/ψ resonances. (c) The invariant mass distribution of the most energetic photon and two kaons. Black markers with error bars show the data in the η signal region. The grey histograms show the data in the η sidebands. The dashed line is the $\chi_{c0,1,2}$ contribution, from the data in the signal region, which are extracted by a global fit (the solid line). Arrows indicate the requirement to exclude the χ_{c2} events.

To investigate possible background contributions, the same analysis is also performed on an inclusive MC sample of 5.06×10^8 $\psi(3686)$ events. The dominant non- η background events come from $\psi(3686) \rightarrow \gamma\chi_{cJ}$ ($J = 0, 1, 2$), $\chi_{cJ} \rightarrow K^+K^-\pi^0$ with a missing photon. We then investigate the invariant mass of the combination of K^+K^- together with the most energetic photon. The χ_{cJ} peaks are clearly evident, as indicated in Fig. 1(c), where the black markers and grey histograms are data from the η signal region and sidebands, respectively. Unlike the $\chi_{c0,1}$ peaks, the χ_{c2} background peak cannot be well estimated with the η mass sidebands ($0.478 < M(\gamma\gamma) < 0.498 \text{ GeV}/c^2$ or $0.598 < M(\gamma\gamma) < 0.618 \text{ GeV}/c^2$). Therefore, the candidate events in the χ_{c2} mass region of $3.54 < M(\gamma_{\max}KK) < 3.58 \text{ GeV}/c^2$ are rejected.

After the above requirements, a sample of 1787 $\psi(3686) \rightarrow K^+K^-\eta$ candidates remains. The Dalitz plot for these events, displayed in Fig. 2, shows some structures in the distribution. Structures are also obvious in the K^+K^- mass spectrum shown in Fig. 3(a), but not in the $K^+\eta$ and $K^-\eta$ mass spectra shown in Fig. 3(b) and Fig. 3(c). Using

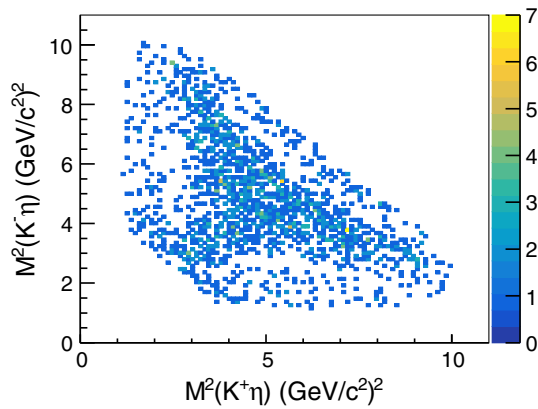


FIG. 2. Dalitz plot for selected $\psi(3686) \rightarrow K^+K^-\eta$ events.

the η mass sidebands, the number of background events is estimated to be 257, as shown by the shaded histograms in Figs. 3(a), (b), and (c), and no evident structures are observed in these background K^+K^- and $K^\pm\eta$ mass spectra.

To investigate possible backgrounds from QED processes, which are produced directly in e^+e^- annihilation rather than in $\psi(3686)$ decays, a study is made using a data sample taken at $\sqrt{s} = 3.773 \text{ GeV}$, with an integrated luminosity of 2.92 fb^{-1} [26]. After normalizing according to integrated luminosities and the $1/s$ dependence of the cross sections, the background contribution from QED processes is estimated to be 27.5 ± 3.1 events. Due to the low statistics, this contribution is only considered in the systematic uncertainty due to background contributions.

IV. PARTIAL WAVE ANALYSIS

A. Analysis method

In the PWA, the decay amplitudes in the sequential decay process $\psi(3686) \rightarrow X\eta$, $X \rightarrow K^+K^-$ and $\psi(3686) \rightarrow X^\mp K^\pm$, $X^\mp \rightarrow K^\mp\eta$ are constructed using the covariant tensor formalism described in Ref. [27]. The general form for the decay amplitude is

$$A = \psi_\mu(m)A^\mu = \psi_\mu(m) \sum_i \Lambda_i U_i^\mu, \quad (1)$$

where $\psi_\mu(m)$ is the polarization vector of the $\psi(3686)$ and m is the spin projection of $\psi(3686)$; U_i^μ is the partial wave amplitude with coupling strength determined by a complex parameter Λ_i . The partial wave amplitudes U_i used in the analysis are constructed with the four momenta of daughter particles according to the expressions given in Ref. [27].

In this analysis, each intermediate resonance is described by a relativistic Breit-Wigner function with an invariant-mass dependent width [28],

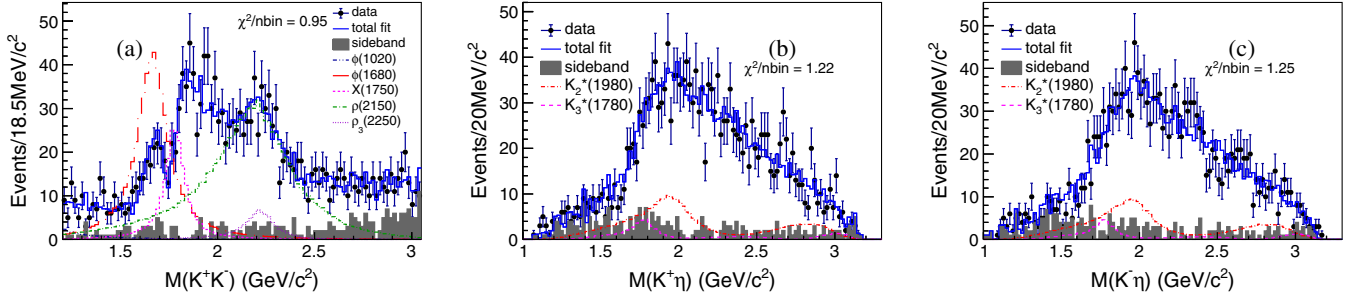


FIG. 3. Comparisons to the fit projections for the (a) K^+K^- , (b) $K^+\eta$, and (c) $K^-\eta$ invariant mass distributions.

$$BW(s) = \frac{1}{m^2 - s - i\sqrt{s}\Gamma(s)}, \quad (2)$$

$$\Gamma(s) = \Gamma_0(m^2) \left(\frac{m^2}{s}\right) \left(\frac{p(s)}{p(m^2)}\right)^{2l+1}, \quad (3)$$

where s is the invariant mass squared of the daughter particles, m and Γ_0 are the mass and width of the intermediate resonance, respectively, l is the orbital angular momentum for a daughter particle, and $p(s)$ or $p(m^2)$ is the momentum of a daughter particle in the rest frame of the resonance with mass \sqrt{s} or m .

The probability to observe the i th event characterized by the measurement ξ_i , i.e., the measured four momenta of the particles in the final state, is

$$P(\xi_i) = \frac{\omega(\xi_i)\varepsilon(\xi_i)}{\int d\Phi \omega(\xi)\varepsilon(\xi)}, \quad (4)$$

where $\omega(\xi_i) \equiv (\frac{d\sigma}{d\Phi})_i$ is the differential cross section, $\varepsilon(\xi_i)$ is the detection efficiency, $d\Phi$ is the standard element of phase space for three-body decays, and $\int d\Phi \omega(\xi)\varepsilon(\xi) = \sigma'$ is the measured total cross section. The differential cross section is given by [27]

$$\omega = \frac{d\sigma}{d\Phi} = \frac{1}{2} \sum_{\mu=1}^2 A^\mu A^{*\mu}, \quad (5)$$

where A^μ is the total amplitude for all possible resonances, and $\mu = 1, 2$ labels the transverse polarization directions. Longitudinal polarization is absent since with highly relativistic beams e^+e^- annihilation produces $\psi(3686)$ with spin projection $J_z = \pm 1$ relative to the beam.

The likelihood for the data sample is

$$\mathcal{L} = \prod_{i=1}^N P(\xi_i) = \prod_{i=1}^N \frac{\omega(\xi_i)\varepsilon(\xi_i)}{\sigma'}. \quad (6)$$

Technically, it is more straightforward to minimize negative log-likelihood (NLL), $\mathcal{S} = -\ln \mathcal{L}$, instead of maximizing \mathcal{L} , with

$$\mathcal{S} = -\ln \mathcal{L} = -\sum_i^N \ln \left(\frac{\omega(\xi_i)}{\sigma'} \right) - \sum_i^N \ln \varepsilon(\xi_i). \quad (7)$$

In Eq. (7), the second term is a constant and has no impact on the determination of the amplitude parameters or on the relative changes in \mathcal{S} . In the fit, $-\ln \mathcal{L}$ is defined as

$$-\ln \mathcal{L} = -\sum_i^N \ln \left(\frac{\omega(\xi_i)}{\sigma'} \right) = -\sum_i^N \ln \omega(\xi_i) + N \ln \sigma'. \quad (8)$$

The complex couplings, i.e., the relative magnitudes and phases, of amplitudes are determined through an unbinned maximum likelihood fit. The resonance parameters are optimized by a scan method. We perform many independent fits with varying initial values but with a specific value of the resonance parameter under study until a stable minimum negative log-likelihood (MNLL) value is obtained. We then scan, performing a series of such MNLL searches with various values for the resonance parameter; the resonance parameter value with the minimum MNLL is taken as our nominal value. For each pair of charge conjugate processes and resonances, the two partners use the same complex coupling and resonance parameters.

The free parameters in the likelihood function are optimized using MINUIT [29]. The measured total cross section σ' is evaluated using a dedicated MC sample consisting of N_{gen} events uniformly distributed in phase space. These events are subjected to the selection criteria described in Sec. III and yield a sample of N_{acc} accepted events. The normalization integral is then computed as

$$\int d\Phi \omega(\xi)\varepsilon(\xi) = \sigma' \rightarrow \frac{1}{N_{\text{gen}}} \sum_k^{N_{\text{acc}}} \omega(\xi_k). \quad (9)$$

The background contribution in the fit is estimated using the η sideband data and is subtracted from the log-likelihood function for data in the η signal region, i.e.,

$$\mathcal{S} = -(\ln \mathcal{L}_{\text{DATA}} - \ln \mathcal{L}_{\text{BG}}). \quad (10)$$

The number of the fitted events N_X for an intermediate resonance X is defined as

$$N_X = \left(\frac{\sigma_X}{\sigma'} \right) N', \quad (11)$$

$$\sigma_X = \frac{1}{N_{\text{gen}}} \sum_{j=1}^{N_{\text{acc}}} \omega_X(\xi_j), \quad (12)$$

where N' is the number of selected events after background subtraction and ω_X denotes the observed differential cross section for the process with the intermediate state X .

The detection efficiency ε_X for the intermediate resonance X is obtained using a weighted MC sample that resembles the data,

$$\varepsilon_X = \frac{\sigma_X}{\sigma_X^{\text{gen}}} = \frac{\sum_{j=1}^{N_{\text{acc}}} \omega_X(\xi_j)}{\sum_{k=1}^{N_{\text{gen}}} \omega_X(\xi_k)}. \quad (13)$$

Taking $\psi(3686) \rightarrow X\eta$, $X \rightarrow K^+K^-$ as an example, the product branching fraction is calculated according to

$$\mathcal{B}(\psi(3686) \rightarrow X\eta, X \rightarrow K^+K^-) = \frac{N_X}{N_\psi \cdot \varepsilon_X \cdot \mathcal{B}(\eta \rightarrow \gamma\gamma)}, \quad (14)$$

where N_ψ is the number of $\psi(3686)$ events [17] and $\mathcal{B}(\eta \rightarrow \gamma\gamma)$ is the branching fraction of $\eta \rightarrow \gamma\gamma$ [23].

The free parameters in the fit are the relative magnitudes and phases of the amplitudes. The statistical uncertainties of the signal yields are propagated from the covariance matrix obtained from the fit. The statistical uncertainties for the masses and widths, which are optimized using a scan method, are defined as one standard deviation from the optimized results, corresponding to a change of 0.5 in the log-likelihood value, for a specific parameter.

The statistical significance of a given intermediate resonance is evaluated using the change in the log-likelihood value and the number of free parameters in the fit with and without the specific resonance.

B. PWA result

A PWA is performed on the accepted 1787 candidate events for $\psi(3686) \rightarrow K^+K^-\eta$, where the background contribution is described with 257 events from the η mass sidebands. Though most of $\psi(3686) \rightarrow \phi\eta$ events are removed by requiring $M(K^+K^-) > 1.2 \text{ GeV}/c^2$, the amplitude for $\psi(3686) \rightarrow \phi\eta$ is included in the PWA to evaluate its impact on the interference between the tail of the ϕ and other components. However, its contribution is constrained to the expected number of events, 24.3 ± 2.4 , which is estimated from the branching fraction of $\psi(3686) \rightarrow \phi\eta$ [23].

TABLE I. Mass, width and significance of each component in the baseline solution. The first uncertainties are statistical and the second are systematic.

Resonance	M (MeV/ c^2)	Γ (MeV)	Significance
$\phi(1680)$	1680_{-13-21}^{+12+21}	185_{-26-47}^{+30+25}	14.3σ
$X(1750)$	1784_{-12-27}^{+12+0}	106_{-19-36}^{+22+8}	10.0σ
$\rho(2150)$	2255_{-18-41}^{+17+50}	$460_{-48-90}^{+54+160}$	23.5σ
$\rho_3(2250)$	2248_{-17-59}^{+17+59}	$185_{-26-103}^{+31+17}$	8.5σ
$K_2^*(1980)$	2046_{-16-15}^{+17+67}	408_{-34-44}^{+38+72}	19.9σ
$K_3^*(1780)$	1813_{-15-16}^{+15+65}	191_{-37-81}^{+43+3}	11.2σ

For the other components in the fit, a large number of attempts are made to evaluate the possible resonance contributions in the K^+K^- and $K^\pm\eta$ mass spectra [30]. Only components with a statistical significance larger than 5σ are kept in the baseline solution. In addition to the ϕ , the baseline fit includes contributions from the $\phi(1680)$, $X(1750)$, $\rho(2150)$, $\rho_3(2250)$, $K_2^*(1980)^\pm$, and $K_3^*(1780)^\pm$. The fit results, including the resonance parameters, the statistical significance and the product branching fraction for each component, are summarized in Table I and Table II. Table III shows the resonance parameters in baseline solution and their average values in Particle Data Group (PDG) [23].

The spin-parity assignment of the baseline solution is checked for each component separately. Replacing $\phi(1680)$, $\rho(2150)$, or $\rho_3(2250)$ by a 3^{--} [1^{--} for $\rho_3(2250)$] resonance with same mass and width worsens the NLL values by 81.8, 213.8, and 40.1, with the number of degrees of freedom unchanged. Altering the $K_2^*(1980)$ spin parity to 1^- , 3^- , 4^+ or the $K_3^*(1780)$ to 1^- , 2^+ , 4^+ worsens the NLL values by at least 40 units. The spin-parity assignment of the $X(1750)$ as 1^{--} is significantly better than the 3^{--} hypothesis, with the NLL values improved by 53.4 units.

The PWA results provide a good description of the data, as illustrated by the comparisons between the fit projections and the data for $M(K^+K^-)$, $M(K^+\eta)$, $M(K^-\eta)$, and angular distributions in Figs. 3 and 4. In addition, the comparisons

TABLE II. Branching fraction for each process in the baseline solution. The first uncertainties are statistical and the second are systematic.

Decay mode	BF ($\times 10^{-6}$)
$\psi(3686) \rightarrow \phi(1680)\eta \rightarrow K^+K^-\eta$	$12.0 \pm 1.3_{-6.9}^{+6.5}$
$\psi(3686) \rightarrow X(1750)\eta \rightarrow K^+K^-\eta$	$4.8 \pm 1.0_{-2.6}^{+2.6}$
$\psi(3686) \rightarrow \rho(2150)\eta \rightarrow K^+K^-\eta$	$21.7 \pm 1.9_{-8.3}^{+7.7}$
$\psi(3686) \rightarrow \rho_3(2250)\eta \rightarrow K^+K^-\eta$	$1.9 \pm 0.4_{-1.3}^{+0.5}$
$\psi(3686) \rightarrow K_2^*(1980)^\pm K^\mp \rightarrow K^+K^-\eta$	$7.0 \pm 0.5_{-0.6}^{+3.7}$
$\psi(3686) \rightarrow K_3^*(1780)^\pm K^\mp \rightarrow K^+K^-\eta$	$2.0 \pm 0.4_{-0.4}^{+1.9}$

TABLE III. Comparison of resonances parameters in the baseline solution and their average values in PDG. The first uncertainties are statistical and the second are systematic.

Resonance	This work		PDG [23]	
	M (MeV/ c^2)	Γ (MeV)	M (MeV/ c^2)	Γ (MeV)
$\phi(1680)$	1680^{+12+21}_{-13-21}	185^{+30+25}_{-26-47}	1680 ± 20	150 ± 50
$X(1750)$	1784^{+12+0}_{-12-27}	106^{+22+8}_{-19-36}	$(1720 \pm 20)_{\rho(1700)}$ $(1753.5 \pm 1.5 \pm 2.3)_{X(1750)}$ [15]	$(250 \pm 100)_{\rho(1700)}$ $(122.2 \pm 6.2 \pm 8.0)_{X(1750)}$ [15]
$\rho(2150)$	2255^{+17+50}_{-18-41}	$460^{+54+160}_{-48-90}$	$(2153 \pm 27)_{\rho(2150)}$ [31] $(2175 \pm 15)_{\phi(2170)}$	$(389 \pm 79)_{\rho(2150)}$ [31] $(61 \pm 18)_{\phi(2170)}$
$\rho_3(2250)$	2248^{+17+59}_{-17-5}	$185^{+31+17}_{-26-103}$	2232 [32]	220 [32]
$K_2^*(1980)$	2046^{+17+67}_{-16-15}	408^{+38+72}_{-34-44}	$1973 \pm 8 \pm 25$	$373 \pm 33 \pm 60$
$K_3^*(1780)$	1813^{+15+65}_{-15-16}	191^{+43+3}_{-37-81}	1776 ± 6	159 ± 21

of the angular distributions for the η (K^\pm) in different center-of-mass frames also indicate the fit projections are consistent with the data.

In the K^+K^- mass spectrum, the apparent structure around 1.7 GeV/ c^2 is identified in the PWA as the well established $\phi(1680)$. The PWA fit gives a mass of 1680^{+12+21}_{-13-21} MeV/ c^2 and a width of 185^{+30+25}_{-26-47} MeV, with a statistical significance of 14.3σ , which are consistent with the world average values of the $\phi(1680)$ [23]. To

describe the clear dip between 1.7 GeV/ c^2 and 1.8 GeV/ c^2 , another vector resonant structure, with a statistical significance of 10.0σ , is included in the PWA. Interestingly, the fitted mass and width of this structure are 1784^{+12+0}_{-12-27} MeV/ c^2 and 106^{+22+8}_{-19-36} MeV, respectively, which are in agreement with those of the $X(1750)$ reported by the FOCUS Collaboration [15]. The $X(1750)$ was originally interpreted as the photoproduction mode of the $\phi(1680)$ [12–14] with the limited statistics. The

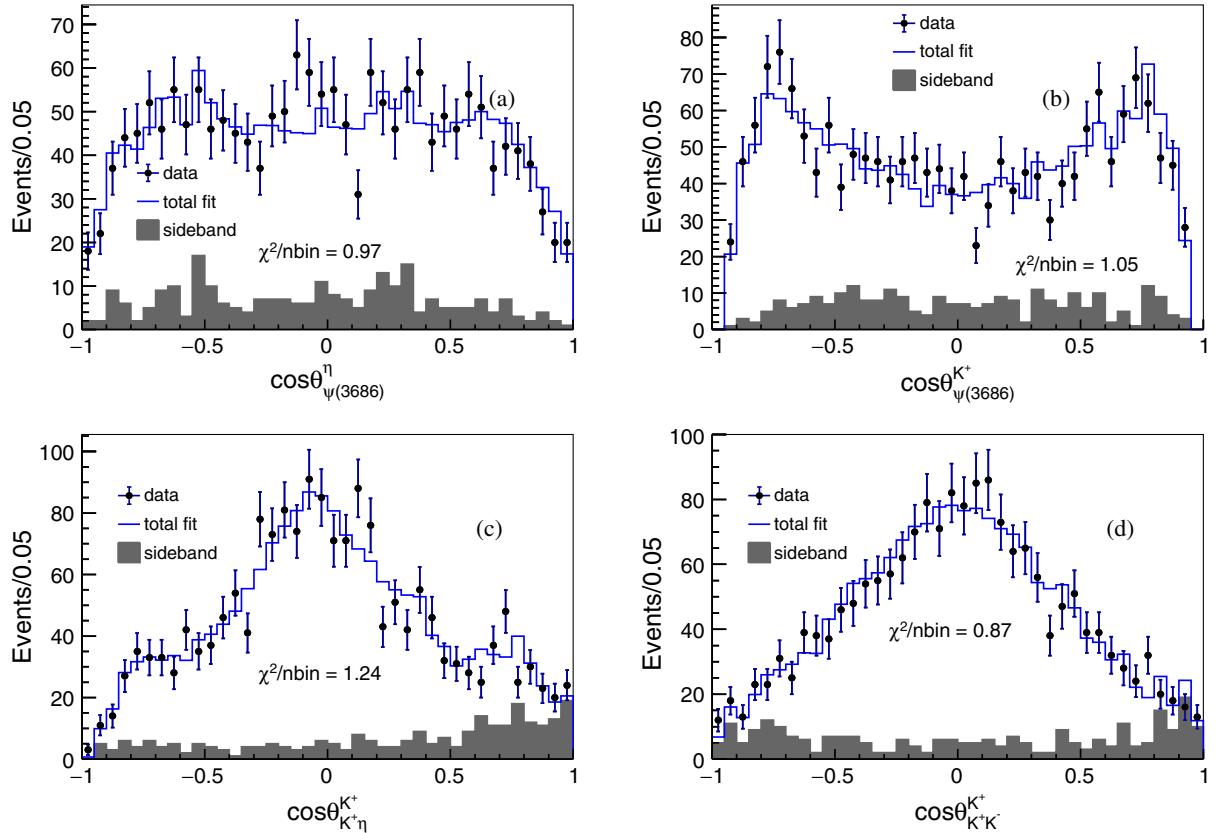


FIG. 4. Fit projections to (a) $\cos \theta$ of the η in the $\psi(3686)$ rest frame, (b) $\cos \theta$ of the K^+ in the $\psi(3686)$ frame, (c) $\cos \theta$ of the K^+ in the $K^+\eta$ rest frame, (d) $\cos \theta$ of the K^+ in the K^+K^- rest frame.

observation of both the $\phi(1680)$ and the $X(1750)$ in the K^+K^- mass spectrum implies that the $X(1750)$ is a new structure instead of the photoproduction mode of the $\phi(1680)$. The $\rho(1700)$ is another 1^{--} resonance in the mass region [1.7, 1.8] GeV/ c^2 . The $\rho(1700)$ has a quite different mass and width compared to the $X(1750)$, as shown in Table III. To distinguish the $X(1750)$ and the $\rho(1700)$, an alternative fit is performed after fixing the mass and width of the observed $X(1750)$ to instead be those of the $\rho(1700)$ [23]. This alternate fit yields a likelihood 5.7σ worse than the nominal fit. This test indicates the observed additional vector resonance is more likely to be the $X(1750)$ than the $\rho(1700)$. However, the $\rho(1700)$ has a very large uncertainty in its mass and width. This large uncertainty of the $\rho(1700)$ prohibits excluding the possibility that this vector structure is the $\rho(1700)$.

Reference [9], which used a subset of the data sample used in this analysis, assumed the structure around 2.2 GeV/ c^2 to be the $\phi(2170)$. By introducing one 1^{--} component, the PWA fit in this analysis gives $M = 2255_{-18-41}^{+17+50}$ MeV/ c^2 and $\Gamma = 460_{-48-90}^{+54+160}$ MeV. The width is much larger than that of the $\phi(2170)$ from previous measurements [3–8,10]. This structure could be either the $\phi(2170)$ or the $\rho(2150)$ or perhaps a superposition of both. To obtain a good description of the angular distribution, we find that an additional resonance with a mass of 2248_{-17-5}^{+17+59} MeV/ c^2 and a width of $185_{-26-103}^{+31+17}$ MeV and $J^{PC} = 3^{--}$ is also necessary, which is interpreted as the $\rho_3(2250)$ because the mass and width are consistent with previous measurements of the $\rho_3(2250)$ [32,33]. Due to the low statistics, the uncertainties on the resonant parameters for these two structures are quite large. Since, for either excited ρ state, $\psi(3686) \rightarrow \rho\eta$ is an isospin violating decay and $\rho \rightarrow K^+K^-$ is suppressed by the OZI rule, the investigation of the $\pi^+\pi^-$ invariant mass in $\psi(3686) \rightarrow \pi^+\pi^-\eta$ may make it possible to establish which of these possibilities is correct.

In the $K^\pm\eta$ mass spectra, the fit results indicate that the dominant contributions come from the established $K_2^*(1980)$ and $K_3^*(1780)$ mesons. The fitted masses and widths of these two resonances, which are summarized in Table I, are consistent with their world average values [23].

V. BRANCHING FRACTION OF $\psi(3686) \rightarrow K^+K^-\eta$

The comparisons of different mass spectra and angular distributions, as displayed in Figs. 3 and 4, indicate that the PWA results are in good agreement with the data. In this case, the PWA results provide a good model to simulate the decay $\psi(3686) \rightarrow K^+K^-\eta$ and allow a determination of its branching fraction with

$$\mathcal{B}(\psi(3686) \rightarrow K^+K^-\eta) \quad (15)$$

$$\begin{aligned} &= \frac{N_{\text{data}} - N_{\text{sd}} - N_{\phi\eta} - N_{\text{QED}}}{N_\psi \mathcal{B}(\eta \rightarrow \gamma\gamma) \varepsilon} \\ &= (3.49 \pm 0.09 \pm 0.15) \times 10^{-5}, \end{aligned} \quad (16)$$

where $N_{\text{data}} = 1787$ is the number of $\psi(3686) \rightarrow K^+K^-\eta$ candidates after excluding $\psi(3686) \rightarrow \phi\eta$ and $\psi(3686) \rightarrow J/\psi\eta$ processes with a requirement $1.20 < M(K^+K^-) < 3.05$ GeV/ c^2 . The background contribution estimated by η sidebands is $N_{\text{sd}} = 257$. Contributions from the remaining $\psi(3686) \rightarrow \phi\eta$ and QED processes are estimated to be $N_{\phi\eta} = 24.3 \pm 2.4$ and $N_{\text{QED}} = 27.5 \pm 3.1$. The detection efficiency is determined to be $\varepsilon = 23.95\%$ modeled by the PWA results above. The first uncertainty is statistical and the second is systematic, which will be discussed below.

VI. SYSTEMATIC UNCERTAINTIES

The systematic uncertainties in the intermediate resonance measurements are divided into two categories. The uncertainties in the first category are applicable to all branching fraction measurements. These uncertainties include the systematic uncertainties from photon detection (1% per photon [34]), MDC tracking (1% per charged track [35]), PID (1% per kaon [36]), number of $\psi(3686)$ events [17], the branching fraction of $\eta \rightarrow \gamma\gamma$ (0.5% [23]), and the kinematic fit (1.4%). The systematic uncertainty associated with the kinematic fit comes from the inconsistency of the track-helix parameters between the data and MC simulation. This difference can be reduced by correcting the helix parameters of charged tracks in the MC simulation as described in Ref. [37]. The uncertainty due to the kinematic fit is estimated to be 1.4% by comparing the detection efficiency with and without the correction.

The uncertainties in the second category are due to the PWA fit procedure and are applicable to measurements of both branching fractions of intermediate states and the corresponding resonance parameters. Sources of these uncertainties include impact from the tail of the $\phi(1020)$ resonance, resonance parametrization, resonance parameters, background estimation (χ_{c2} veto, contribution from QED processes, and sideband region), additional resonances, and the radius of the centrifugal barrier. These uncertainties are discussed below.

- (i) χ_{c2} veto: In the nominal fit, events within the window $3.54 < M(\gamma_{\text{max}}KK) < 3.58$ GeV/ c^2 are removed. To estimate the uncertainty due to this requirement, these events are included in the fit, and a MC sample of $\psi(3686) \rightarrow \gamma\chi_{c2}, \chi_{c2} \rightarrow K^+K^-\pi^0$ is used to describe χ_{c2} background in the fit. The MC events are generated in accordance with the amplitude analysis results in Ref. [38] to provide a good description of the data. The differences in the PWA fit results due to this change are taken as uncertainties. The change of the branching fraction of $\psi(3686) \rightarrow K^+K^-\eta$, 1.1%, with and without this

TABLE IV. Sources of systematic uncertainties and their corresponding contributions to the mass (in MeV/ c^2) and width (in MeV) of intermediate resonances.

Sources	$\phi(1680)$		$X(1750)$		$\rho(2150)$		$\rho_3(2250)$		$K_2^*(1980)^\pm$		$K_3^*(1780)^\pm$	
	ΔM	$\Delta\Gamma$	ΔM	$\Delta\Gamma$	ΔM	$\Delta\Gamma$	ΔM	$\Delta\Gamma$	ΔM	$\Delta\Gamma$	ΔM	$\Delta\Gamma$
Breit-Wigner parametrization	+14.4	-14.3	+0.3	-15.3	+34.9	+70.9	+39.8	+2.5	+54.1	+67.7	+54.1	+0.2
Resonance parameter	+6.0 -15.7	+13.4 -22.0	-9.1	-22.0	+8.2 -8.1	+13.0 -21.9	+13.6	+2.7 -49.8	+9.2 -10.4	+20.1 -20.9	+6.2 -10.4	+1.1 -40.3
χ_{c2} veto	-3.2	+1.3	-9.9	-2.3	-2.9	+5.2	+24.9	-62.6	+12.6	+11.7	-0.9	-20.9
Background estimation	-10.3	-6.0	-3.7	-18.5	-14.7	+131.2	+1.7	-51.7	-7.7	-31.5	+5.5	-43.4
Continuum background	-3.7	-1.6	-6.9	-8.3	+1.0	-4.4	+9.4	-24.3	+1.5	+1.7	-0.7	-7.2
Additional resonances	+14.5	+11.0 -33.2	-20.3	+8.1 -4.6	+25.2 -28.2	+43.9 -48.9	+25.9	+16.1 -15.8	+33.3 -6.7	-18.8	+33.4 -6.7	+2.2 -42.1
Barrier radius	-6.8	+17.9 -18.5	-9.5	-11.2	+24.7 -24.1	+32.6 -71.9	+19.1 -5.0	-27.1	+16.3	+4.4 -13.4	+12.2 -9.8	+0.3 -28.0
Total	+21.3 -20.6	+25.0 -46.6	+0.3 -27.3	+8.1 -35.8	+50.3 -40.8	+159.5 -89.8	+59.3 -5.0	+16.5 -103.2	+67.4 -14.6	+71.7 -44.3	+65.3 -15.8	+2.5 -80.9

requirement is assigned as the uncertainty from this source.

- (ii) Sideband region: The events in the η sideband region ($0.478 < M(\gamma\gamma) < 0.498$ GeV/ c^2 or $0.598 < M(\gamma\gamma) < 0.618$ GeV/ c^2) are used to estimate the background contribution in the PWA fit. An alternative sideband region ($0.488 < M(\gamma\gamma) < 0.508$ GeV/ c^2 or $0.588 < M(\gamma\gamma) < 0.608$ GeV/ c^2) is also used and the differences in the fit results relative to the nominal ones are taken as the associated uncertainties.
- (iii) The tail of the $\phi(1020)$ resonance: The $\phi(1020)$ resonance is very narrow and is far away from the PWA region. Impacts from the tail of the $\phi(1020)$, the resolution effect on the $\phi(1020)$ tail and the uncertainty of the branching fraction $\psi(3686) \rightarrow \phi(1020)\eta$, are negligible. As a test, we artificially increase the width of the $\phi(1020)$ to 6.27 MeV [$\sim 1.5 \times \Gamma(\phi)$] and refit data. The difference between this result and the nominal result

is found to be negligible. We also vary the branching fraction of $\psi(3686) \rightarrow \phi(1020)\eta$ by $\pm 1\sigma$ around the world average value in the fit and comparing these fit results with the nominal result. Differences due to variations of the branching fraction are found to be negligible.

- (iv) Resonance parametrization: To estimate the uncertainty due to the resonance parametrization of the resonance shape, we performed the PWA by replacing the nominal parametrization with a relativistic Breit-Wigner with a constant width [27] $f = \frac{1}{m^2 - s - im\Gamma}$, where m and Γ are the mass and width of the resonance, and s is the invariant mass squared of the daughter particles. The differences due to the resonance parametrization are taken as the systematic uncertainties.
- (v) Resonance parameters: The uncertainty due to resonance parameters (mass and width) is estimated by varying the parameters by $\pm 1\sigma$ around the

TABLE V. Sources of systematic uncertainties and their corresponding contributions (in %) to the branching fraction for each decay process.

Sources	$\phi(1680)$	$X(1750)$	$\rho(2150)$	$\rho_3(2250)$	$K_2^*(1980)^\pm$	$K_3^*(1780)^\pm$	$\psi(3686) \rightarrow K^+K^-\eta$
Photon detection	2.0	2.0	2.0	2.0	2.0	2.0	2.0
MDC tracking	2.0	2.0	2.0	2.0	2.0	2.0	2.0
Particle ID	2.0	2.0	2.0	2.0	2.0	2.0	2.0
Kinematic fit	1.4	1.4	1.4	1.4	1.4	1.4	1.4
$\mathcal{B}(\eta \rightarrow \gamma\gamma)$	0.5	0.5	0.5	0.5	0.5	0.5	0.5
Number of $\psi(3686)$ events	0.6	0.6	0.6	0.6	0.6	0.6	0.6
χ_{c2} veto	-18.2	-20.2	-8.8	+5.7	-5.9	-14.1	1.1
Background estimation	-31.7	-3.5	-27.9	-1.4	+25.3	+7.0	1.4
Breit-Wigner parametrization	+2.8	+8.5	-8.6	+6.1	+14.0	+5.2	...
Resonance parameter	+53.7 -30.5	+49.4 -35.8	+10.9 -7.8	+12.7 -14.5	+8.5 -3.0	+8.9 -6.8	...
Continuum background	-5.7	+7.9	-0.9	+6.6	+0.2	+6.5	...
Additional resonances	-29.3	-36.2	+16.6 -14.7	+18.5 -60.4	+41.9	+93.0 -9.1	...
Barrier radius	+5.3 -12.2	+21.5	+29.4 -15.8	+11.6 -28.9	+7.1 -5.0	+11.8	...
Total	+54.2 -57.6	+55.2 -55.0	+35.7 -38.4	+27.7 -68.6	+52.2 -9.1	+94.8 -18.5	4.2

nominal results in the fit, one at a time. The largest changes after these variations are taken as the systematic uncertainties.

- (vi) QED contribution: The estimated contribution from QED processes is 27.5 ± 3.1 events, which are not included in the nominal fit. The uncertainty is estimated by subtracting this contribution using a datalike MC sample, which includes $K_2^*(1430)^+K^- + \text{c.c.}$, $K_3^*(1780)^+K^- + \text{c.c.}$ and 1^{--} nonresonant processes. The MC sample is generated according to a preliminary PWA fit to the 2.92 fb^{-1} data sample taken at 3.773 GeV [26]. The differences between the nominal fit and the fit with the QED contribution subtracted are taken as systematic uncertainties.
- (vii) Additional resonances: To estimate uncertainties due to additional resonances, fits with additional resonances are performed. The spin 1 resonances $K^*(1410)$ (4.3σ), $K^*(1680)$ (3.9σ), and spin 3 resonance $\rho_3(1990)$ (2.2σ) [23] are included separately. The differences relative to the nominal result are taken as systematic uncertainties.
- (viii) Radius of the centrifugal barrier: The Blatt-Weisskopf barrier factor [39,40] is included in the PWA decay amplitudes and the radius (R) of the centrifugal barrier is used in the factor via $Q_0 = (0.197321/R[\text{fm}]) \text{ GeV}/c$ [27]. In the nominal fit Q_0 is set to $0.2708 \text{ GeV}/c$. Fits with alternative radii ($Q_0 = 0.15 \text{ GeV}/c$, and $Q_0 = 0.5 \text{ GeV}/c$) are also performed and the differences relative to the nominal fit result are taken as systematic uncertainties.

Systematic uncertainties for masses, widths and branching fractions and the sources described above are summarized in Table IV and Table V. Assuming all the above uncertainties are independent, the total systematic uncertainty is calculated by adding them in quadrature.

VII. SUMMARY

Using a sample of 4.48×10^8 $\psi(3686)$ events collected with the BESIII detector, we perform a partial wave analysis of $\psi(3686) \rightarrow K^+K^-\eta$ for the first time. After excluding contributions from $\psi(3686) \rightarrow \phi\eta$ and $\psi(3686) \rightarrow J/\psi\eta$ processes, the branching fraction of $\mathcal{B}(\psi(3686) \rightarrow K^+K^-\eta)$ is calculated to be $(3.49 \pm 0.09 \pm 0.15) \times 10^{-5}$. With the advantage of the higher statistics data set and the precision MC model, this result is in agreement with but more precision than the previous measurement [9]. This measurement supersedes that in Ref. [9] which was based on a subsample of the data used in this work.

In the K^+K^- mass spectrum, in addition to the established $\phi(1680)$, a 1^{--} state is necessary to describe the dip around $1.75 \text{ GeV}/c^2$, which is caused by the interference between the two states. The fitted mass and width of the

1^{--} resonance are consistent with those of the $X(1750)$ reported by the FOCUS Collaboration [15]. However, due to the large uncertainty in the mass and width of the $\rho(1700)$, the possibility that this 1^{--} resonance is the $\rho(1700)$ cannot be excluded. The broad structure around $2.2 \text{ GeV}/c^2$ is caused by contributions from a broad 1^{--} structure and a 3^{--} structure. The likely candidate for the former state is either the $\phi(2170)$, $\rho(2150)$, or a superposition of both, while the latter state may be attributed to the $\rho_3(2250)$. However, it is still difficult to distinguish these states from the excited ϕ and ρ states due to the limited statistics. With the help of other decays, e.g., $\psi(3686) \rightarrow \pi^+\pi^-\eta$, a combined partial wave analysis may help to distinguish these states as strangeonium or excited ρ states.

In the $K^\pm\eta$ mass spectra, no clear peak is observed. The partial wave analysis finds that the dominant K^* contributions are from two known states, the $K_2^*(1980)$ and $K_3^*(1780)$.

ACKNOWLEDGMENTS

The BESIII Collaboration thanks the staff of BEPCII and the IHEP computing center for their strong support. This work is supported in part by National Key Basic Research Program of China under Contract No. 2015CB856700; National Natural Science Foundation of China (NSFC) under Contracts No. 11521505, No. 11625523, No. 11635010, No. 11675184, No. 11735014; National Natural Science Foundation of China (NSFC) under Contract No. 11835012; National Key Research and Development Program of China No. 2017YFB0203200; the Chinese Academy of Sciences (CAS) Large-Scale Scientific Facility Program; Joint Large-Scale Scientific Facility Funds of the NSFC and CAS under Contracts No. U1532257, No. U1532258, No. U1732263, No. U1832207; CAS Key Research Program of Frontier Sciences under Contracts No. QYZDJ-SSW-SLH003, No. QYZDJ-SSW-SLH040; Chinese Academy of Science Focused Science Grant; National 1000 Talents Program of China; 100 Talents Program of CAS; INPAC and Shanghai Key Laboratory for Particle Physics and Cosmology; German Research Foundation DFG under Contract No. Collaborative Research Center CRC 1044, FOR 2359; Istituto Nazionale di Fisica Nucleare, Italy; Koninklijke Nederlandse Akademie van Wetenschappen (KNAW) under Contract No. 530-4CDP03; Ministry of Development of Turkey under Contract No. DPT2006K-120470; National Science and Technology fund; The Knut and Alice Wallenberg Foundation (Sweden) under Contract No. 2016.0157; The Royal Society, UK under Contract No. DH160214; The Swedish Research Council; U.S. Department of Energy under Contracts No. DE-FG02-05ER41374, No. DE-SC-0010118, No. DE-SC-0012069; University of Groningen (RuG) and the Helmholtzzentrum fuer Schwerionenforschung GmbH (GSI), Darmstadt.

- [1] S. Godfrey and N. Isgur, *Phys. Rev. D* **32**, 189 (1985).
- [2] T. Barnes, N. Black, and P.R. Page, *Phys. Rev. D* **68**, 054014 (2003).
- [3] B. Aubert *et al.* (BABAR Collaboration), *Phys. Rev. D* **74**, 091103 (2006).
- [4] B. Aubert *et al.* (BABAR Collaboration), *Phys. Rev. D* **76**, 012008 (2007).
- [5] B. Aubert *et al.* (BABAR Collaboration), *Phys. Rev. D* **77**, 092002 (2008).
- [6] C. P. Shen *et al.* (Belle Collaboration), *Phys. Rev. D* **80**, 031101 (2009).
- [7] J. P. Lees *et al.* (BABAR Collaboration), *Phys. Rev. D* **86**, 012008 (2012).
- [8] M. Ablikim *et al.* (BES Collaboration), *Phys. Rev. Lett.* **100**, 102003 (2008).
- [9] M. Ablikim *et al.* (BESIII Collaboration), *Phys. Rev. D* **86**, 072011 (2012).
- [10] M. Ablikim *et al.* (BESIII Collaboration), *Phys. Rev. D* **91**, 052017 (2015).
- [11] M. Ablikim *et al.* (BESIII Collaboration), *Phys. Rev. D* **100**, 032004 (2019).
- [12] J. Busenitz *et al.* (Fermilab E401 Collaboration), *Phys. Rev. D* **40**, 1 (1989).
- [13] M. Atkinson *et al.* (Omega Photon Collaboration), *Z. Phys. C* **27**, 233 (1985).
- [14] D. Aston *et al.* (Omega Photon Collaboration), *Phys. Lett.* **104B**, 231 (1981).
- [15] J. M. Link *et al.* (FOCUS Collaboration), *Phys. Lett. B* **545**, 50 (2002).
- [16] P. L. Liu, S. S. Fang, and X. C. Lou, *Chin. Phys. C* **39**, 082001 (2015).
- [17] M. Ablikim *et al.* (BESIII Collaboration), *Chin. Phys. C* **42**, 023001 (2018).
- [18] M. Ablikim *et al.* (BESIII Collaboration), *Nucl. Instrum. Methods Phys. Res., Sect. A* **614**, 345 (2010).
- [19] C. H. Yu *et al.*, *Proceedings of IPAC2016, Busan, Korea* (JACoW, Geneva, Switzerland, 2016), <http://accelconf.web.cern.ch/AccelConf/ipac2016/doi/JACoW-IPAC2016-TUYA01.html>.
- [20] S. Agostinelli *et al.* (GEANT4 Collaboration), *Nucl. Instrum. Methods Phys. Res., Sect. A* **506**, 250 (2003).
- [21] S. Jadach, B. F. L. Ward, and Z. Was, *Phys. Rev. D* **63**, 113009 (2001); *Comput. Phys. Commun.* **130**, 260 (2000).
- [22] D. J. Lange, *Nucl. Instrum. Methods Phys. Res., Sect. A* **462**, 152 (2001); R. G. Ping, *Chin. Phys. C* **32**, 599 (2008).
- [23] C. Patrignani *et al.* (Particle Data Group), *Chin. Phys. C* **40**, 100001 (2016).
- [24] J. C. Chen, G. S. Huang, X. R. Qi, D. H. Zhang, and Y. S. Zhu, *Phys. Rev. D* **62**, 034003 (2000); R. L. Yang, R. G. Ping, and H. Chen, *Chin. Phys. Lett.* **31**, 061301 (2014).
- [25] E. Richter-Was, *Phys. Lett. B* **303**, 163 (1993).
- [26] M. Ablikim (BESIII Collaboration), *Chin. Phys. C* **37**, 123001 (2013).
- [27] B. S. Zou and D. V. Bugg, *Eur. Phys. J. A* **16**, 537 (2003).
- [28] J. H. Kuhn and A. Santamaria, *Z. Phys. C* **48**, 445 (1990).
- [29] F. James and M. Roos, *Comput. Phys. Commun.* **10**, 343 (1975).
- [30] Resonances tested but excluded from the baseline solution due to low significance: $K^*(1410)^\pm$, $K^*(1680)^\pm$, $K_2^*(1430)^\pm$, $K_4^*(2045)^\pm$, $\omega(1420)$, $\rho(1450)$, $\rho(1570)$, $\omega(1650)$, $\rho(1900)$, $\omega_3(1670)$, $\rho_3(1690)$, $\phi_3(1850)$, $\rho_3(1990)$.
- [31] M. E. Biagini, S. Dubnicka, E. Etim, and P. Kolar, *Nuovo Cimento A* **104**, 363 (1991).
- [32] A. Hasan and D. V. Bugg, *Phys. Lett. B* **334**, 215 (1994).
- [33] A. V. Anisovich, C. A. Baker, C. J. Batty, D. V. Bugg, L. Montanet, V. A. Nikonov, A. V. Sarantsev, V. V. Sarantsev, and B. S. Zou, *Phys. Lett. B* **542**, 8 (2002).
- [34] M. Ablikim *et al.* (BESIII Collaboration), *Phys. Rev. D* **81**, 052005 (2010).
- [35] M. Ablikim *et al.* (BESIII Collaboration), *Phys. Rev. D* **85**, 092012 (2012).
- [36] M. Ablikim *et al.* (BESIII Collaboration), *Phys. Rev. D* **99**, 112010 (2019).
- [37] M. Ablikim *et al.* (BESIII Collaboration), *Phys. Rev. D* **87**, 012002 (2013).
- [38] M. Ablikim *et al.* (BESIII Collaboration), *Phys. Rev. D* **96**, 111102 (2017).
- [39] S. U. Chung, *Phys. Rev. D* **48**, 1225 (1993); **57**, 431 (1998).
- [40] F. von Hippel and C. Quigg, *Phys. Rev. D* **5**, 624 (1972).